Atmos. Chem. Phys., 9, 4797–4810, 2009
www.atmos-chem-phys.net/9/4797/2009/
© Author(s) 2009. This work is distributed under
the Creative Commons Attribution 3.0 License.

Atmospheric Chemistry and Physics

First year of upper tropospheric integrated content of CO_2 from IASI hyperspectral infrared observations

C. Crevoisier[1], **A. Chédin**[1], **H. Matsueda**[2], **T. Machida**[3], **R. Armante**[1], **and N. A. Scott**[1]

[1]Laboratoire de Météorologie Dynamique/CNRS/IPSL, Ecole Polytechnique, Palaiseau, France
[2]Geochemical Research Department, Meteorological Research Institute, Tsukuba, Japan
[3]Center for Global Environmental Research, National Institute for Environmental Studies, Tsukuba, Japan

Received: 5 March 2009 – Published in Atmos. Chem. Phys. Discuss.: 27 March 2009
Revised: 30 June 2009 – Accepted: 16 July 2009 – Published: 21 July 2009

Abstract. Simultaneous observations from the Infrared Atmospheric Sounding Interferometer (IASI) and from the Advanced Microwave Sounding Unit (AMSU), launched together onboard the European MetOp platform in October 2006, are used to retrieve an upper tropospheric content of carbon dioxide (CO_2) covering the range 11–15 km (100–300 hPa), in clear-sky conditions, in the tropics, over sea, for the first year of operation of MetOp (January 2008–December 2008). With its very high spectral resolution, IASI provides fourteen channels in the 15 μm band highly sensitive to CO_2 with reduced sensitivities to other atmospheric variables. IASI observations, sensitive to both CO_2 and temperature, are used in conjunction with AMSU observations, only sensitive to temperature, to decorrelate both signals through a non-linear inference scheme based on neural networks. A key point of this approach is that no use is made of prior information in terms of CO_2 seasonality, trend, or geographical patterns. The precision of the retrieval is estimated to be about 2.0 ppmv ($\sim$0.5%) for a $5^\circ \times 5^\circ$ spatial resolution on a monthly time scale. Features of the retrieved CO_2 space-time distribution include: (1) a strong seasonal cycle of 4 ppmv in the northern tropics with a maximum in June–July and a minimum in September–October. This cycle is characterized by a backward two-months lag as compared to the surface, by a backward one-month lag as compared to measurements performed at 11 km, and by a forward one-month lag as compared to observations performed at the tropopause (16 km). This is likely due to the time-lag of CO_2 cycle while transported from the surface to the upper troposphere; (2) a more complex seasonal cycle in the southern tropics, in agreement with in-situ measurements; (3) a latitudinal variation of CO_2 shifting from a South-to-North increase of 3.5 ppmv in boreal spring to a South-to-North decrease of 1.5 ppmv in the fall, in excellent agreement with tropospheric aircraft measurements; (4) signatures of CO_2 emissions transported to the upper troposphere. In addition to bringing an improved view of CO_2 distribution, these results from IASI should provide an additional means to observe and understand atmospheric transport pathways of CO_2 from the surface to the upper troposphere.

Correspondence to: C. Crevoisier
(cyril.crevoisier@lmd.polytechnique.fr)

1 Introduction

Knowledge of today's carbon sources and sinks, their spatial distribution and their variability in time is one of the essential ingredients for predicting the future carbon dioxide (CO_2) atmospheric concentration levels, and in turn radiative forcing of climate change by CO_2. The distribution of atmospheric CO_2 reflects both spatial and temporal evolutions as well as the magnitude of surface fluxes (Tans et al., 1990). The traditional atmospheric top-down approach (e.g. Gurney et al., 2004) uses atmospheric transport models to determine the spatio-temporal land-air surface flux distribution that gives the best match to a global set of atmospheric CO_2 data. In principle, it is thus possible to estimate these fluxes from atmospheric CO_2 concentration, provided that atmospheric transport can be accurately modeled. However, this approach is currently limited by the sparse and uneven distribution of the global flask sampling programs. Moreover, it requires an

Published by Copernicus Publications on behalf of the European Geosciences Union.

accurate modeling of atmospheric transport, which still suffers from limitation, especially along the vertical (Stephens et al., 2007; Yang et al., 2007). Densely sampling the atmosphere in time and space, satellite measurements of the distribution of global atmospheric CO_2 concentration could in principle provide a way to address both issues.

Until the recent launch of JAXA/GOSAT on 23 January 2009, which is the first space mission specifically designed for CO_2 monitoring, information on CO_2 atmospheric distribution came first from thermal infrared sounders (Chédin et al., 2002, 2003; Crevoisier et al., 2004; Engelen et al., 2004; Chahine et al., 2005; Maddy et al., 2008; Strow and Hannon, 2008), and then from near infrared remote sensing (Buchwitz et al., 2005; Barkley et al., 2007; Schneising et al., 2008). Infrared sounders, which rely on thermal contrast to infer trace gas concentrations, perform best in the middle to upper troposphere. They thus bring limited information on surface fluxes, and attempts to use retrievals to constrain atmospheric inversions of CO_2 surface fluxes have been for the most part unsuccessful (Chevallier et al., 2005). This is partly due to biases affecting the satellite retrievals that are hard to correctly assess, but also to the difficulties of models to reproduce vertical transport, and hence, middle tropospheric CO_2 variability (Tiwari et al., 2006; Shia et al., 2006; Yang et al., 2007; Stephens et al., 2007). Although only sensitive to CO_2 in the mid-to-upper troposphere, thermal infrared sounders, used alone or in combination with new near-infrared spaceborne instruments that bring information on the total column, may thus give a better constraint on the model transport and vertical mixing in top-down flux estimation. They can also give valuable information on specific signals such as CO_2 fire emissions uplifted to the part of the atmosphere seen by the sounders (Chédin et al., 2008).

Although infrared sounders have historically been designed for meteorological soundings (temperature, water vapor, ozone), the impact of CO_2 variations can be seen on some satellite records, in particular temperature estimated from infrared observations made in CO_2 absorption bands (e.g. Turner, 1993, 1994). The first interpretation of infrared radiances in terms of CO_2 concentration were performed by Chédin et al. (2002), yielding the first observation of the year-to-year increase of CO_2 from space. Chédin et al. (2002) used observations from the Television and Infrared Operational Satellite-Next Generation (TIROS-N) Operational Vertical Sounder (TOVS), flown aboard the National Oceanic and Atmospheric Administration (NOAA) polar meteorological satellites since 1978. The authors analyzed the differences between the satellite observations and simulations from a radiative transfer model using collocated radiosonde data and fixed gas concentration as the prime input to derive seasonal cycles and trends of CO_2, N_2O and CO in three latitudinal bands. Its main limit was its dependency upon collocations between satellite observations and radiosonde measurements because of their inability to measure all necessary information (surface temperatures, upper stratospheric temperatures, etc.) and the uneven distribution of the radiosonde stations.

The main difficulty in estimating global distribution of CO_2 from infrared sounders comes from the fact that CO_2 infrared measurements are sensitive to both temperature and CO_2 variations. Independent information on temperature is thus needed to allow separating these two effects. Chédin et al. (2003) used a non linear inference scheme based on neural network to differentiate between temperature and CO_2 by including Microwave Sounding Unit (MSU) radiances in the process, since microwave radiance are insensitive to CO_2 but not to temperature. Four years of mid-to-upper tropospheric CO_2 content covering the 1987–1991 time frame between 20° latitude was retrieved, with a measurement standard deviations of about 3 ppm. The authors also successfully retrieved mean CO_2 growth rates over the $\pm 20°$ latitude range of 1.75 ppm/year that agreed quite well with in situ measurements. Accuracy of the retrievals from this first generation of infrared sounders was however limited by the low spectral resolution of the TOVS instruments, and by the lack of channels only sensitive to CO_2.

The launch of the Atmospheric Infrared Sounder (AIRS) and of the Advanced Microwave Sounding Unit (AMSU) onboard NASA/Aqua satellite in May 2002 brought a new step in the monitoring of trace gases from space, and several studies presented CO_2 estimates from AIRS. Crevoisier et al. (2004) extended the stand-alone approach developed by Chédin et al. (2003) to derive a mid-to-upper tropospheric content of CO_2, using the Aqua/AMSU microwave observations to bring the necessary information on atmospheric temperature. The measurement standard deviation was about 2.5 ppm. Engelen and McNally (2005) proposed a one-dimensional variational data assimilation system, which has recently been extended to a full four-dimensional system (Engelen et al., 2009) relying on the European Center for Medium-range Weather Forecasts (ECMWF) Integrated Forecast System (IFS). Chahine et al. (2005, 2008) used a classic linear estimation scheme to retrieve an upper-tropospheric content of CO_2. Maddy et al. (2008) used a regularized nonlinear least squares solution, and relied on AIRS retrieved atmospheric temperature and other thermodynamic variables. Finally, Strow and Hannon (2008) used a least-squares method based on a few AIRS channels specifically sensitive to the lower troposphere, and relied on ECMWF analyses for the atmospheric temperature profile. The major limitation of all these studies comes from the information on atmospheric temperature. For studies relying on meteorological analyses or retrieved temperature profiles, uncertainty in these variables, and possible errors in cloud-clearing (as opposed to cloud-screening) significantly impact the precision of the retrieved CO_2; for estimation schemes based on the use of AMSU channels, the high radiometric noise of Aqua/AMSU channel 7, which is the only channel purely sensitive to troposphere, degrades the precision of the retrievals. Moreover, for the studies based on optimal

techniques relying on a first guest, the impact of the choice of this first guess on the retrieved CO_2 is usually not fully assessed.

With its 8461 channels covering most of the infrared spectrum at a very high spectral resolution, the Infrared Atmospheric Sounding Interferometer (IASI) launched onboard the European MetOp platform in October 2006, gives the opportunity to use several channels specifically sensitive to CO_2. Moreover, the Advanced Microwave Sounding Unit (AMSU) also flying onboard MetOp provides microwave observations that cover the whole atmospheric column with satisfactory radiometric characteristics. The goal of this paper is to present and evaluate the first retrieval of an upper tropospheric integrated content of carbon dioxide from MetOp IASI/AMSU observations for the year 2008. This study is focused on the tropical belt (20° N:20° S) where higher-quality retrievals are expected compared to the extratropics because of the low variability of the temperature profiles. Section 2 describes data and modeling tools used in the retrieval process. Section 3 presents the selection of IASI channels based on their sensitivity to CO_2 and other atmospheric variables, along with the non-linear inference scheme used to retrieve a tropospheric integrated content of CO_2. Section 4 describes the retrievals in terms of seasonal cycle, latitudinal variations and geographical distribution, which are compared to airborne measurements. Section 5 gives the conclusion.

2 Data and modeling tools

2.1 Satellite data: IASI, AMSU and HIRS4

The Infrared Atmospheric Sounding Interferometer (IASI) developed by the Centre National d'Etudes Spatiales (CNES) in collaboration with the European Organisation for the Exploitation of Meteorological Satellites (EUMETSAT) is a Fourier Transform Spectrometer based on a Michelson Interferometer coupled to an integrated imaging system that measures infrared radiation emitted from the Earth. IASI provides 8461 spectral samples, aligned in three bands between 645.0 cm^{-1} and 2760 cm^{-1} (15.5 μm and 3.63 μm), with a spectral resolution of 0.5 cm^{-1} after apodisation ("Level 1c" spectra). The spectral sampling interval is 0.25 cm^{-1}. IASI is an across track scanning system with scan range of $\pm 48.3°$, symmetrically with respect to the nadir direction. A nominal scan line covers 30 scan positions towards the Earth. The instantaneous field of view (IFOV) has a ground resolution of 12 km at nadir.

Also flying onboard MetOp, the Advanced Microwave Sounding Unit (AMSU) is a cross-track scanning total-power radiometer with 15 channels that measure scene radiance in the microwave spectrum from 23.8 to 89.0 GHz. The AMSU instrument has an IFOV of 48 km at nadir, with scan range of $\pm 48.3°$ from nadir with a total of 30 Earth fields-of-view per scan line. The swath width is approximately 2000 km.

Finally, the MetOp/High-Resolution Infrared Radiation Sounder (HIRS-4) measures atmospheric and/or surface emission in seven channels located around 15.0 μm, five located around 4.3 μm, and an 11.0 μm window channel. Ozone emission is measured in a 9.6 μm channel. Other channels measure water vapor emission around 7 μm and surface emission at shorter wavelengths, around 4 μm. Its observations will be used in this study for cloud-screening.

IASI Level 1c, and AMSU and HIRS4 Level 1b data are routinely archived at LMD via the Centre for Atmospheric Chemistry Products and Services Ether website (http://ether.ipsl.jussieu.fr/), through EUMETCast, the Broadcast System for Environmental Data of EUMETSAT.

2.2 Radiative models and data: 4A and TIGR

Infrared radiative simulations used in this study are performed using the fast line-by-line 4A (Automatized Atmospheric Absorption Atlas) model (Scott and Chédin, 1981; http://ara.lmd.polytechnique.fr/; http://www.noveltis.fr/4AOP/). Co-developed by the Laboratoire de Météorologie Dynamique (LMD) and NOVELTIS with the support of CNES, 4A is the reference radiative transfer model for the CNES/EUMETSAT IASI Level 1 Cal/Val and operational processing. Here, it uses spectroscopy from the regularly updated GEISA (Gestion et Etude des Informations Spectroscopiques Atmosphériques: Management and Study of Spectroscopic Information) spectral line data catalog (Jacquinet-Husson et al., 2008).

Our study is based on a statistically representative description of the atmosphere from the Thermodynamic Initial Guess Retrieval (TIGR) database (Chédin et al., 1985), with associated radiative information. Use is made of a version of TIGR (F. Chevallier, personal communication, 2008) which comprises 7490 tropical atmospheric situations (4425 over sea, the remaining over land), each of them described by its profiles of temperature, water vapour and ozone. CO_2, CH_4, CO and N_2O reference concentrations are assumed constant along the vertical at 372 ppmv, 1860 ppbv, 100 ppbv and 324 ppbv, respectively. For all TIGR atmospheric situations, for all scan angles, and for the 8461 IASI channels (about 10^9 cases all together), clear-sky brightness temperatures (BT), transmittances and Jacobians (partial derivative of the channel BT with respect to a layer physical variable such as a gas mixing ratio, a temperature or the emissivity) are computed using 4A. The 15 AMSU BT are computed using the in house STRANSAC microwave forward model.

The noise due to the instrument is also computed using the following equation

$$NE\Delta T\,(\nu, T_B(\nu)) = NE\Delta T\,(\nu, T_{\mathrm{ref}})\,\frac{\frac{\partial B}{\partial T}\,(\nu, T_{\mathrm{ref}})}{\frac{\partial B}{\partial T}\,(\nu, T_B(\nu))} \qquad (1)$$

where $NE\Delta T$ is the equivalent noise temperature taken at the brightness temperature T_B, of the channel located at

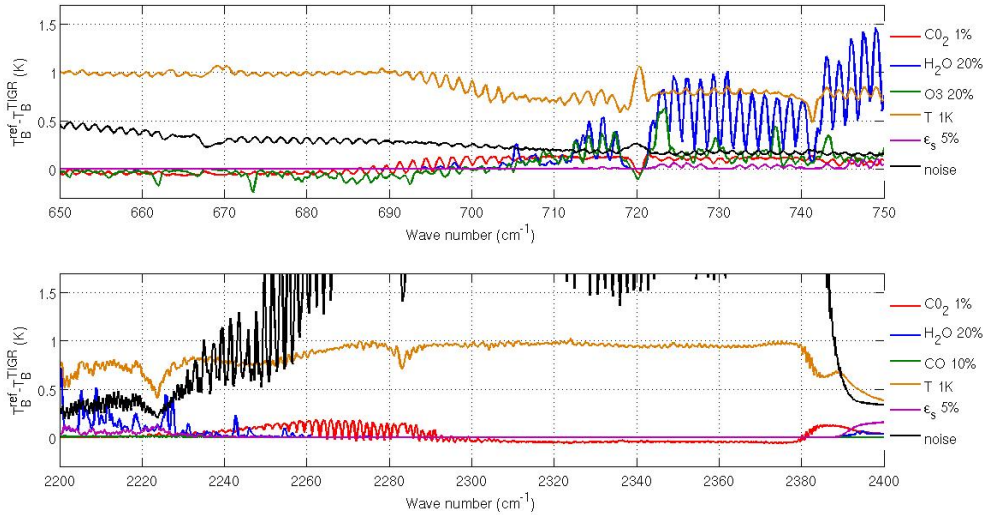

Fig. 1. Sensitivities of IASI channels located in the 15 μm (top) and 4.3 μm (bottom) bands to variations of carbon dioxide (1%), water vapor (20%), ozone (20%) carbon monoxide (10%), atmospheric temperature (1 K), and surface emissivity (0.05), and instrument noise computed at the brightness temperature. Average over the TIGR tropical atmospheric situations.

frequency ν, and B is the radiance. The reference noise corresponding to a reference temperature T_{ref} of 280 K is taken from the in-flight noise measurement (CNES, personal communication, 2008).

3 CO_2 retrieval method

3.1 Channel selection: sensitivity study of IASI channels

CO_2-sensitive channels are located in two spectral bands, one located around 15 μm (700 cm^{-1}) in the ν_2 branch, and one located around 4.3 μm (2000 cm^{-1}) in the ν_3 branch. They present various sensitivities to carbon dioxide and other atmospheric or surface components. The first problem arising in the retrieval method is thus the choice of a set of channels presenting the best properties regarding the retrieval of CO_2. As described in Crevoisier et al. (2003a), three criteria must be used to reach this goal: (1) the sensitivity of the channels to atmospheric CO_2 changes; (2) the sensitivity of the channels to other gases or thermodynamic variables of the atmosphere; (3) the part of the atmosphere to which the channels are sensitive to CO_2 variations.

In the 15 μm band, channels are sensitive to water vapor (H_2O), ozone (O_3) and surface characteristics; in the 4.3 μm band, channels are sensitive to H_2O, carbon monoxide (CO), and surface characteristics (emissivity and temperature). The corresponding variations, averaged over the TIGR tropical atmospheric situations, are plotted in Fig. 1 in terms of variation of the measured brightness temperature for a variation of 1 K for atmospheric temperature, 1% for CO_2, 20% for H_2O, 20% for O_3, 10% for CO, and 0.05 for surface emissivity. The radiometric noise computed at the BT of the scene is also plotted in Fig. 1.

In both bands, some regions present negative signals (around 650 cm^{-1} or 2350 cm^{-1}). They are regions where the channels essentially look in the stratosphere. By contrast, channels located in regions presenting a positive signal essentially look in the troposphere. The variations of brightness temperature due to CO_2 are the same in both spectral bands, about 0.1 K for a 1% variation of CO_2 atmospheric concentration. However, channels located near 4.3 μm are less sensitive to other atmospheric components, which should, in principle, facilitate the retrieval of CO_2 by increasing the signal-to-inteference ratio. Unfortunately, the IASI radiometric noise is higher in the shortwave than in the longwave, and can be more than twenty times higher than the CO_2 signal in the shortwave region. This precludes using the channels located in the 4.3 μm band. In the following, only channels located in the 15 μm band will be considered. Since the signal is only at the level of detectability, and despite the spectral averaging implied by the use of many channels, an averaging of the retrievals will be necessary.

In the longwave CO_2 absorption band, channels located beyond 705 cm^{-1} are more and more sensitive to water vapor. Since water vapor variability is quite high, especially in the tropics, and knowledge of its tropospheric distribution still limited, separating CO_2 signal from water vapor is quite challenging and precludes using these channels. Another interference as far as CO_2 is concerned comes from tropospheric ozone, which presents a high variability, and a seasonal cycle which shows similarities with that of CO_2. Hence, channels sensitive to both CO_2 and O_3 must be discarded. The remaining channels are mostly located below

Table 1. List of IASI channels selected to retrieve CO_2. Columns 3 to 9 indicate the sensitivity (in K) of each channel to the variation of CO_2 (1%), H_2O (20%), O_3 (20%), atmospheric temperature (1 K), and surface emissivity (0.05). Column 9 gives the radiometric noise computed at the observed brightness temperature (in K). Column 10 gives the pressure Pmax (hPa) of the maximum of the CO_2 Jacobians.

Channel	ω (cm^{-1})	CO_2 (K)	H_2O (K)	O_3 (K)	T (K)	ϵ_{surf} (K)	Noise (K)	P_{max} (hPa)
199	694.50	0.11	−0.02	0.00	0.88	0.00	0.26	181
205	696.00	0.12	0.00	0.00	0.85	0.00	0.25	211
211	697.50	0.12	0.01	0.00	0.83	0.00	0.24	211
212	697.75	0.12	0.02	0.00	0.82	0.00	0.24	211
218	699.25	0.13	0.02	0.00	0.78	0.00	0.22	235
219	699.50	0.12	0.01	0.00	0.79	0.00	0.22	211
224	700.75	0.12	0.00	0.00	0.74	0.00	0.22	235
225	701.00	0.12	0.02	0.00	0.76	0.00	0.22	235
226	701.25	0.12	0.03	0.00	0.78	0.00	0.22	235
230	702.25	0.12	0.00	0.00	0.69	0.00	0.22	235
231	702.50	0.12	0.01	0.00	0.71	0.00	0.22	235
232	702.75	0.13	0.02	0.00	0.73	0.00	0.22	235
237	704.00	0.12	0.01	0.00	0.70	0.00	0.21	262
238	704.25	0.11	0.01	0.00	0.74	0.00	0.21	262

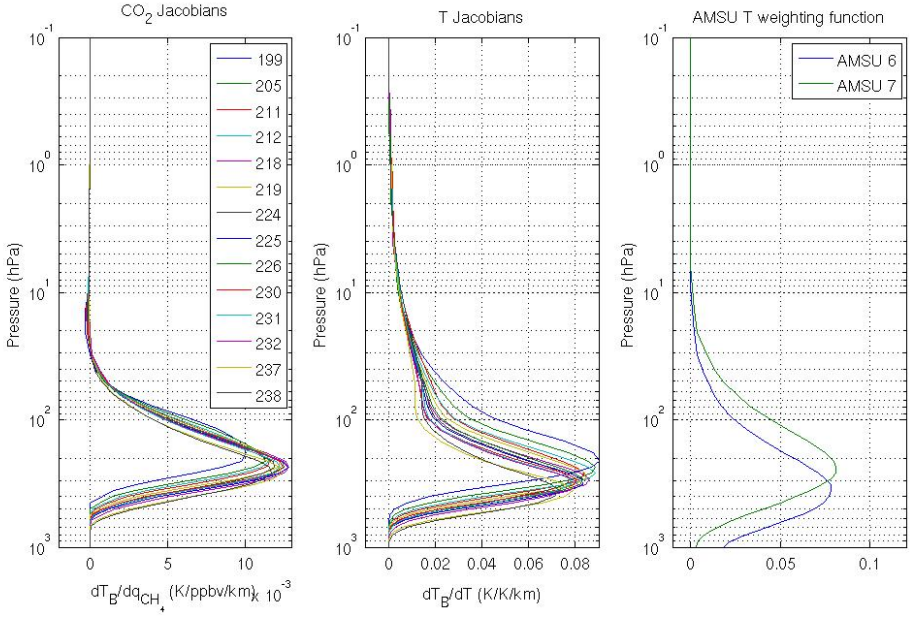

Fig. 2. CO_2 (left) and temperature (middle) Jacobians of the 14 IASI channels selected to estimate carbon dioxide, and (right) AMSU temperature weighting functions. Average over the TIGR tropical atmospheric situations.

705 cm^{-1}. Among them, we have selected 14 channels, which associate the highest sensitivity to CO_2 to almost no interference from other species. They are given in Table 1, along with their sensitivities and altitude of the maximum of their associated CO_2 Jacobians.

CO_2 Jacobians of the 14 selected channels are plotted in Fig. 2. They have very similar shapes and all peak around 200 hPa. Hence, IASI allows the retrieval of a mid-to-upper tropospheric integrated content of carbon dioxide. As seen in Fig. 2, longwave infrared channels sensitive to variations of CO_2 in the troposphere are quite insensitive to two specific regions of the atmosphere: the lower troposphere (roughly below 400 hPa) and the tropopause (Crevoisier et al., 2003a). Indeed, for the lower troposphere, an increase of CO_2 decreases the emission by the surface and increases the emission by the atmosphere: the two terms compensate one another. On the other hand, a channel peaking around the tropopause generally mixes two parts of the temperature

profile, one with a positive slope and one with a negative slope. Once again, an increase of CO_2 gives two signals compensating one another.

As seen on Figs. 1 and 2, infrared CO_2 sensitive channels are intrinsically sensitive to temperature. Greenhouse gases, like CO_2, CH_4, N_2O or CO, have a significant but minor impact, difficult to separate from this dominant signal. A good a priori knowledge of the temperature field may, in principle, be given either by retrievals from IASI, or by NWP reanalysis. However, the noise associated with these fields, at least 1.0 K, makes this information useless for our purpose. In addition, climate-correlated biases associated with retrieved temperatures are particularly difficult to quantify and, thus, to eliminate. This explains why we have chosen to use simultaneous AMSU microwave measurements, only sensitive to temperature, together with IASI infrared measurements, sensitive to both temperature and CO_2 variations, to separate these two effects. As shown in Fig. 2d, AMSU channels 6 and 7 have the temperature weighting functions closest to those of the selected IASI channels, with no sensitivity to the surface. They will be used in the retrieval procedure.

3.2 A non-linear inference scheme

The weakness of the signal induced on IASI brightness temperature (BT) by CO_2 variations, associated with the complexity (in particular its non-Gaussian behavior and the low signal-to-noise ratio) of the relationship between CO_2 concentration and observed BT, makes it difficult to solve this inverse problem. Therefore, a non-linear inference method, based on the Multilayer Perceptron (MLP) neural network (Rumelhart et al., 1986) with two hidden layers, has been preferred to a more classical one. A similar technique has been used to derive tropospheric CO_2 integrated content from TOVS (Chédin et al., 2003, 2008) and AIRS (Crevoisier et al., 2004), and has been successfully applied to the estimation of methane from IASI (Crevoisier et al., 2009).

3.2.1 Neural network

The Multilayer Perceptron (MLP) network is a non-linear mapping model composed of parallel processors called neurons, which are organized in distinct layers. The first layer represents the input of the mapping. The intermediate layers are called the hidden layers. These layers are connected via neural links: two neurons i and j between two consecutive layers have synaptic connections associated with a synaptic weight ω_{ij}. Each neuron j executes two simple operations. First it makes a weighted sum of its N x_i inputs; this sum is then transported through a so-called "transfer function", from which the non-linearity comes from in the model. Here use is made of the classical sigmoidal function

$$\sigma(x) = \tanh(x) \tag{2}$$

The output z_j of neuron j in the hidden layer is thus given by

$$z_j = \sigma\left(\sum_{i=1}^{N} \omega_{ij} x_i\right) \tag{3}$$

Given a neural architecture, defined by a specified number of layers, neurons and connections, all the information of the network is contained in the overall set W of synaptic weights ω_{ij}. The learning algorithm is the optimization technique that estimates the optimal network parameters W by minimizing a positive-definite cost function which measures, for a set of representative situations for which inputs (here the brightness temperatures) and outputs (CO_2) are known (the learning set), the mismatch between the neural network outputs and the desired outputs. Here, the Error Back-Propagation algorithm (Rumelhart et al., 1986) is used to minimize the cost function. It is a gradient descent algorithm well adapted to the MLP hierarchical architecture because the computational cost is linearly related to the number of parameters. To avoid being trapped in local minima during the minimization of the cost function, stochastic steepest descent is used. The learning step is made sample by sample, chosen iteratively and stochastically in the learning data set.

3.2.2 Application to AMSU/IASI observations

The chosen neural architecture is the following. The input layer is composed of: (1) the 14 IASI BT of the tropospheric channels given in Table 1, (2) 2 AMSU BT of channels 6 and 7, and (3) 6 differences between IASI and AMSU 7 BT, to help constraining the convergence process. All together, there are 22 predictors. The output layer of the network is composed of: (1) the difference between the "true" value of CO_2 concentration (associated with inputs) and the "reference" one (372 ppbv), and (2) 14 differences between the "true" IASI BT (associated with the true CO_2 concentration value) and the "reference" one (associated with the reference CO_2 concentration value), once again to constrain the solution. All together, there are 15 predictands. Our past experience and several trials have led us to chose 70 neurons for the first hidden layer and 40 for the second one.

The TIGR database (see Sect. 2.2) is used as the training set from which the networks learn the relationship existing between inputs and outputs. Network input BT correspond to randomly drawn values of CO_2 concentration in the range 362–382 ppmv and are computed from the reference value in TIGR using the CO_2 Jacobians. It is worth noting that no prior information is thus given to the networks in terms of seasonality, trend, or geographical patterns of CO_2.

To avoid the saturation of the neurons composing the first and last layers, which would stem from the shape of the activation function and prevent an efficient learning phase, the input and output data are normalized.

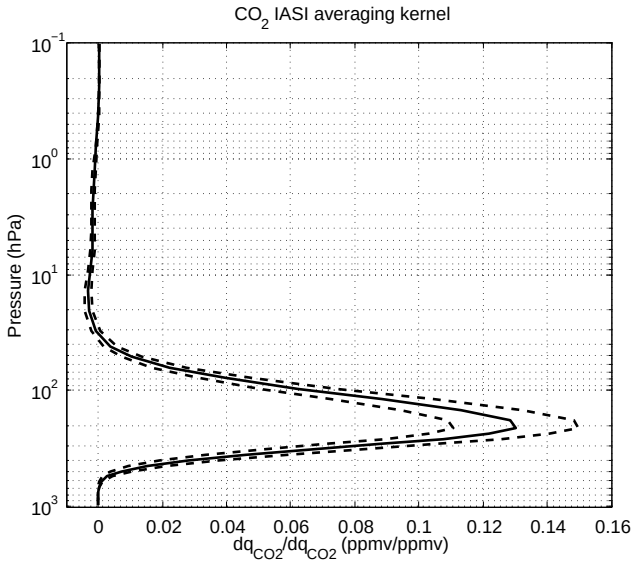

Fig. 3. Averaging kernel of CO_2 IASI retrieval. Mean (full line) plus or minus standard deviation (dashed lines) over the TIGR tropical atmospheric situations.

Use is made of the Error Back-Propagation learning algorithm (Rumelhart et al., 1986), with stochastic steepest descent. At each step of the learning phase, the instrument noise is taken into account by adding to the BT of each channel a random Gaussian noise, which takes into account the radiometric noise and the noise due to inaccuracies in radiative transfer simulations. The radiometric noise is characterized by the equivalent noise temperature ($NE\Delta T$) computed at the BT of the channel according to Eq. (1). To increase the signal to noise ratio, and speed the learning phase, we have chosen to divide the infrared noise by 2. This requires using the average of the 4 IASI BT contained in each single AMSU field-of-view as inputs to the networks. Hence, retrievals will be performed at the AMSU spatial resolution. A total of 7 MLPs have been trained, one for each of the first seven AMSU local zenithal angle, ranging from nadir to an upper limit of 40° to avoid the edges of the orbits.

As stated before, IASI channels are mostly sensitive to mid-to-upper tropospheric variations of CO_2. The averaging kernels, which indicate which part of the atmosphere the retrievals are representative of, are determined through radiative transfer simulations based on the TIGR atmospheric profiles not used in the training of the neural networks. A uniform perturbation of CO_2 mixing ratio is applied sequentially to each of the 39 layers of the atmospheric profiles. IASI and AMSU brightness temperatures are then computed for each of the perturbed atmospheric profiles and used as inputs of the neural network. The theoretical change F_i in ppmv/ppmv of the column mean apparent mixing ratio ($\hat{q}$) given a mixing ratio perturbation of Δq^{ref} at level i, is then given by

$$F_i = \frac{\hat{q}\left(\Delta q_i = \Delta q^{\text{ref}}\right) - \hat{q}\left(\Delta q_i = 0\right)}{\Delta q^{\text{ref}}} \quad (4)$$

The mean and standard deviation of the averaging kernel for the IASI CO_2 retrieval is plotted in Fig. 3. In the tropics, the height of the tropopause being approximately 17 km, the non linear inference scheme gives access to an upper tropospheric integrated content of CO_2 covering the range 100–300 hPa (roughly 11–15 km), with the highest sensitivity around 210 hPa.

3.3 Radiative bias removal

The MLPs are trained with simulated data. Therefore, before presenting observations to the networks, potential radiative systematic biases existing between simulations and observations must be removed. For each channel, the bias is obtained by averaging, over the first year of operation (July 2007–August 2008) and over the whole tropics (20° S:20° N), the differences between simulations, based on the forward model used (assuming a constant profile of CO_2, which is the TIGR reference used to train the network) and radiosonde measurements from the ECMWF ERA-40 database, and collocated (in time and space) satellite observations. Their values are given in Table 2.

3.4 Clear-sky detection

Only clear-sky situations are used to retrieve CO_2. In the absence of a dedicated IASI cloud screening (presently under development), clouds are detected at the MetOp/HIRS4 spatial resolution by a succession of several multispectral threshold tests, stemming from the detection scheme developed for TOVS (Stubenrauch et al., 1998) and AIRS (Crevoisier et al., 2003b). All together, 11 screening tests, detailed in Table 3, are used: (1) 5 tests use differences between BT of HIRS4 and AMSU channels, the latter being almost not sensitive to clouds; (2) 5 tests use differences between window channels, to help detecting low clouds that could still contaminate tropospheric channels; and (3) 1 test, applied to each HIRS FOV, consists in analyzing the standard deviation of BT of channel 8 computed over the 9 closest neighbors; this test is used to measure the heterogeneity of the scene. For the 10 tests based on BT differences, the threshold values are determined respectively to the position of the maximum and the general shape of the histograms of each difference, determined by season, and by angle of view. Their values are given in Table 3. As a result, in the tropics, over sea, during night, about 75% of the situations are found not-clear.

4 Results and discussion

AMSU channel 6 is modestly, though significantly, sensitive to surface, and particularly to relief. Hence, performing the retrievals over land would require a more detailed study of

Table 2. Radiative biases of IASI and AMSU channels used in the retrieval, computed over sea for the first year of MetOp operation.

	IASI														AMSU	
#	199	205	211	212	218	219	224	225	226	230	231	232	237	238	6	7
Bias (K)	1.07	0.86	0.62	0.80	0.54	0.85	0.42	0.63	0.84	0.29	0.51	0.80	0.30	0.47	0.74	0.70

Table 3. Cloud detection tests. $T_B(4)$-$T_B(A7)$ stands for HIRS channel 4 brightness temperature minus AMSU channel 7 brightness temperature. Threshold values are given with regards to the maximum of each test histograms over the season.

	Channels	Min. threshold (K)	Max. threshold (K)	Purpose
HIRS-AMSU	$T_B(4)$-$T_B(A7)$	−1.5	1.2	High/Middle cloud
	$T_B(5)$-$T_B(A6)$	−1.6	1.4	Middle cloud
	$T_B(6)$-$T_B(A5)$	−2.8	2.1	Low cloud
	$T_B(14)$-$T_B(A4)$	−3.2	2.7	Low cloud
	$T_B(15)$-$T_B(A5)$	−1.6	1.4	Low cloud
HIRS-HIRS	$T_B(8)$-$T_B(10)$	−3.3	3.6	Low cloud
	$T_B(4)$-$T_B(5)$	−1.4	3.0	Middle cloud
	$T_B(5)$-$T_B(6)$	−1.3	1.5	Middle/Low cloud
	$T_B(6)$-$T_B(7)$	−1.7	2.1	Low cloud
	$T_B(10)$-$T_B(18)$	−99.0	3.5	Low cloud
HIRS 8: Standard deviation over the 9 closest neightbors < 1.7 K				Heterogeneity test

the influence of surface elevation: so far, the present application is limited to sea cases. CO_2 upper tropospheric integrated content with sensitivity given by the averaging kernel plotted in Fig. 3 is retrieved for the first year of coupled IASI/AMSU observations from January to December 2008.

4.1 Seasonal cycle

As seen in Fig. 4, a clear seasonal cycle of about 4 ppmv is retrieved by IASI in the northern tropics, with a maximum in summer (June–July), and a minimum in the fall (September–October). A slight decrease of the cycle amplitude with latitudes is also observed, in agreement with in-situ measurements (Matsueda et al., 2002) and previous CO_2 retrievals from TOVS (Chédin et al., 2003). Figure 5 shows the average CO_2 seasonal cycle over 2003–2007 measured at six stations from the GLOBALVIEW-CO_2 (2008) network: MLO (19.53° N, 155.57° W, 3.4 km), RPB (13.17° N, 59.43° W, 45 m), CHR (1.70° N, 157.17° W, 3 m), SEY (4.67° S, 55.17° E, 3 m), SMO (14.24° S, 170.57° W, 42 m), and CFA (19.28° S, 147.06° E, 2 m). Compared to surface measurements made in the northern tropics, the amplitude of the IASI retrieved cycle is lower, by about 2 ppmv, and is lagged by 1–2 months (at the surface, CO_2 is at its maximum in April–May and at its minimum in September–October), highlighting the progressive delay of the CO_2 cycle while it is transported upward to the upper troposphere (see below). In the southern tropics, the CO_2 variation is more complex, with a two-maxima structure in spring and summer, and still a minimum in the fall. The amplitude of CO_2 variability in the Southern Hemisphere is also much smaller than in the northern tropics.

Valuable information about CO_2 variations in the middle troposphere is given by regular in-situ measurements of CO_2 made by commercial airliners of the Japan Airlines (JAL) between Japan and Australia since the mid 1980s (Nakazawa et al., 1991; Matsueda et al., 2002; data available at http://gaw.kishou.go.jp/wdcgg.html). In November 2005, the National Institute for Environmental Studies (NIES), the Meteorological Research Institute (MRI), Tohoku University, and Japan Airlines started a new phase of the JAL project called Comprehensive Observation Network for Trace gases by AIrLiner (CONTRAIL), expanding the commercial aircraft measurement program to include regular JAL flights from Japan to Europe, North America, and Asia. In the CONTRAIL project, a newly developed Continuous Measuring Equipment (CME) for in-situ CO_2 observation, as well as an improved Automatic air Sampling Equipment (ASE) for flask sampling have been installed on Boeing 747-400 and Boeing 777-200ER (Machida et al., 2007, 2008; Matsueda et al., 2008; Sawa et al., 2008).

The seasonal cycles of CO_2 measured by JAL/CONTRAIL are plotted in Fig. 6 for the period 2003–2007. IASI retrieved CO_2 cycles are also plotted in Fig. 6 (thick black line). There is a good agreement between both datasets in terms of the cycle amplitude. However, there is a one-month lag between aircraft measurements and IASI retrievals, as shown with the black-dashed line, which

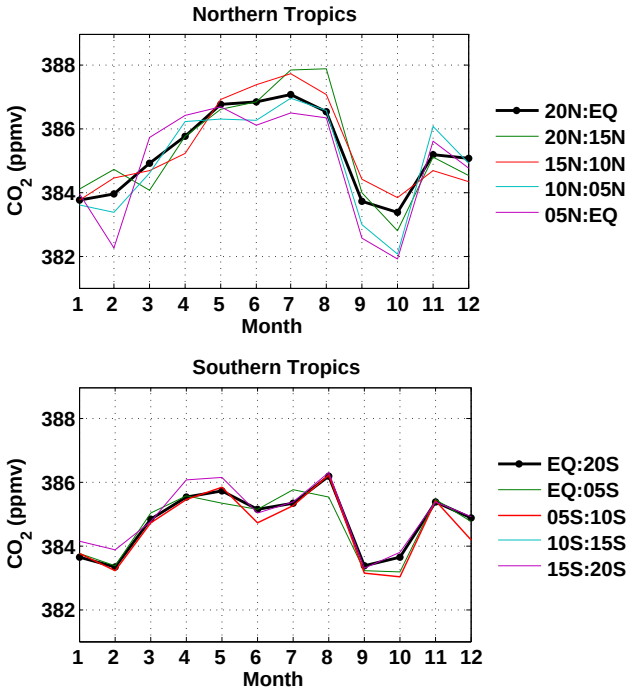

Fig. 4. Seasonal cycle of CO_2 as retrieved in the mid-to-upper troposphere from IASI over the Pacific Ocean in 8 latitudinal bands of 5° each from January 2008 to December 2008 in the northern tropics (top) and southern tropics (bottom). The black line shows the average over the whole band.

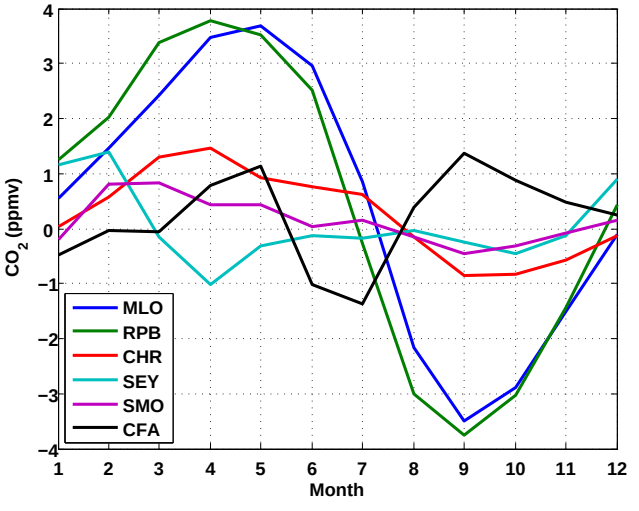

Fig. 5. Seasonal cycle of detrended CO_2 as measured at the surface at six stations from the GLOBALVIEW-CO_2 (2008) network (average over 2004–2007).

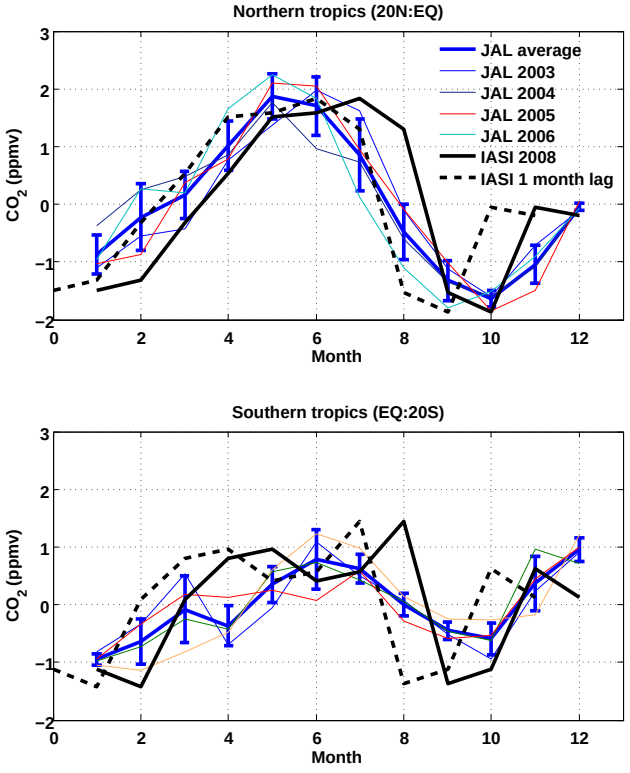

Fig. 6. Seasonal cycle of detrended CO_2 averaged over the northern tropics (top) and the southern tropics (bottom). Thin lines give the JAL/CONTRAIL CO_2 measured by aircraft from 2003 to 2006. The blue thick line gives the JAL/CONTRAIL average of CO_2 over 2003–2006 and associated standard deviation. The thick black line gives the cycle retrieved by IASI (same as in Fig. 4). The thick-dashed black line gives the IASI cycle lagged forward by one-month.

corresponds to the IASI retrieved cycle lagged forward by one month. This lag is likely due to vertical transport of CO_2. Indeed, on one hand, the JAL/CONTRAIL observations cover the altitude range 9–11 km, which corresponds to the lower part of the atmosphere (∼300 hPa) to which selected IASI channels are sensitive, as shown by the CO_2 averaging kernel in Fig. 3. At that altitude, CO_2 is at its maximum in May–June and at its minimum in September–October. On the other hand, several studies (e.g. Boering et al., 1996; Strahan et al., 1998, 2007) have shown that, at the entering point of the stratosphere, the seasonal cycle of CO_2 was lagged backward by 2–3 months as compared to the cycle measured at the surface, with a maximum in July and a minimum in December. In the tropics, the typical entering point of the stratosphere is at 100 hPa, which corresponds to the higher part of the atmosphere to which selected IASI channels are sensitive, as shown by the CO_2 averaging kernel in Fig. 3. Hence, a lag in the IASI retrieved CO_2 cycle of one-month backward as compared to mid-troposphere aircraft measurements on one hand, and of one-month forward as compared to the stratospheric entering air on the other hand seems realistic. This feature was not seen on AIRS retrievals performed previously with a similar estimation scheme (Crevoisier et al., 2004). This might be explained

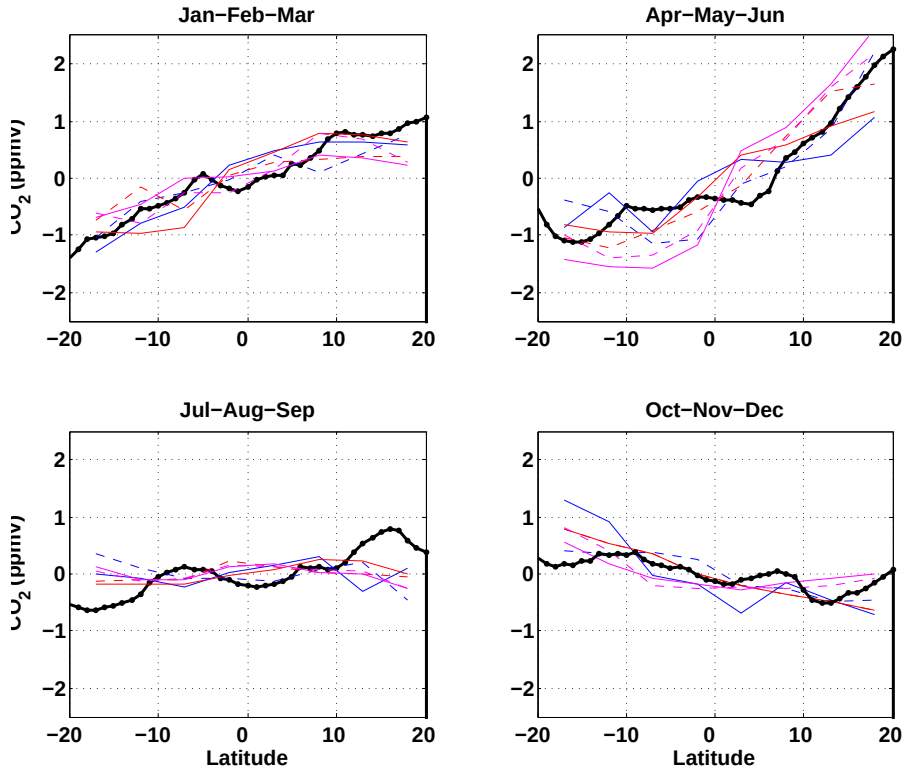

Fig. 7. Latitudinal variation of detrended CO_2 as retrieved from IASI in the mid-to-high troposphere in 2008 (black line) and as measured by JAL airliners at ∼11 km in 2004 (blue lines), 2005 (red lines), and 2006 (purple lines). For the latter dataset, the full (dashed) lines present the average of JAL/CONTRAIL measurements performed at the beginning (end) of the months.

by the use of 15 μm channels only for IASI, whereas both 15 μm and 4.3 μm channels were used for AIRS. As seen in Sect. 3.1, 4.3 μm channels bring information on CO_2 at lower altitude than 15 μm channels. IASI, which is sensitive to the altitude range 100–300 hPa (11–15 km), thus retrieves CO_2 in a higher part of the atmosphere than AIRS, which is sensitive to the altitude range 100–500 hPa (5–15 km).

4.2 Geographic distribution

South-to-North (S–N) CO_2 dependence, as retrieved by IASI in 2008 in a longitudinal band extending from 135° E to 180° E (to have enough items in a region characterized by a large cloudiness), and as observed by JAL/CONTRAIL aircrafts in 2003–2006 around 150° E are plotted for each month in Fig. 7. There is an overall good agreement between IASI retrievals and JAL measurements. The latitudinal variation of atmospheric CO_2 results from the convolution of CO_2 sources and sinks characteristics, CO_2 seasonal variability in the boundary layer, vertical transport and interhemispheric transport. This explains the shift from a S–N increase in the spring to a S–N decrease in winter, which is particularly well captured by IASI. In January–March, in the Northern Hemisphere, the boundary layer CO_2, which started increasing in the fall, keeps growing, but, due to upward transport delay, the S–N increase only starts appearing in the upper troposphere, as seen on both JAL measurements and IASI retrievals. In April–June, CO_2 has reached its maximum in the boundary layer in the Northern Hemisphere, leading to a S–N gradient of about 4 ppmv in the mid-to-upper troposphere. During the drawdown of CO_2 in July–September, the northern CO_2 decreases sharply, yielding an almost constant tropospheric CO_2 in the tropical band. In October–December, while CO_2 starts increasing again in the boundary layer in the Northern Hemisphere, the tropospheric CO_2 remains higher in the southern tropics.

Maps of seasonal mean CO_2 concentration are shown in Fig. 8 from January to December 2008, at a spatial resolution of 5°×5° (1°×1° moving average). This resolution was chosen to average enough individual retrievals to make robust statistics. After the removal of not-clear observations, the number of individual retrievals, per month and per 5°×5° gridbox, is about 400 in regions where clear-sky is prevailing but can be as low as 10 in more cloudy areas. To eliminate possible undetected clouds, boxes having less than 40 individual retrievals are not considered (blank areas on Fig. 8). They mostly correspond to regions of deep convection with persistent cloudiness.

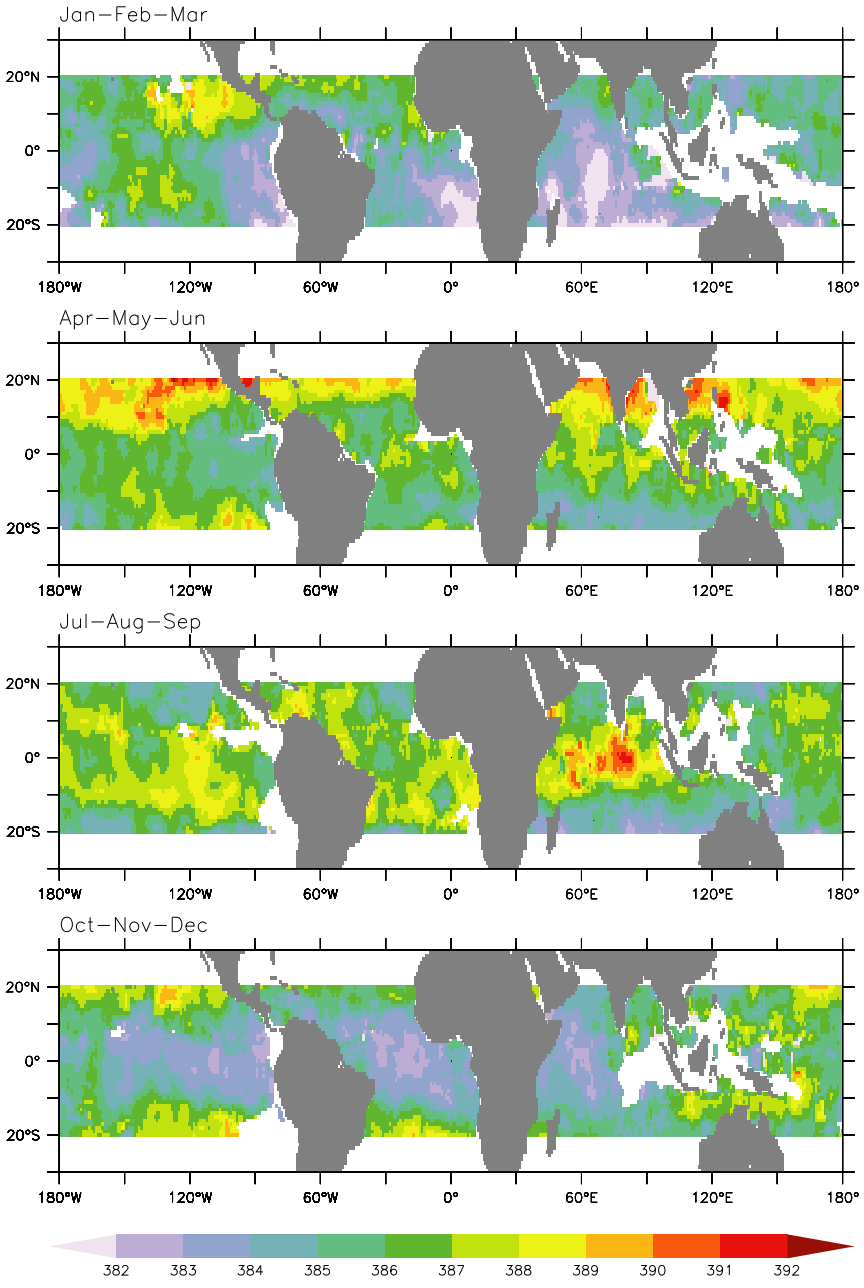

Fig. 8. Seasonal upper tropospheric integrated content of CO_2 (ppmv) as retrieved from IASI observations, from January 2008 to December 2008, at a resolution of $5° \times 5°$. Blank areas denote rejections due to persistent cloudiness.

The seasonal variation of CO_2 concentration is well seen on Fig. 8, especially in the Northern Hemisphere, and follows the one shown in Fig. 6. In Spring, higher concentrations are found in northern tropics. A decrease of these high concentrations is observed during Summer, probably due to the increase of photosynthesis activities of the northern biomass. The shift from a S–N latitudinal CO_2 increase in boreal winter and spring to a S–N decrease in the fall, with a neutral S–N variation in summer is also well retrieved by IASI. As expected, the maximum of variability is found in Spring (April and May), whereas autumnal months (September, October) show a relatively low variability of CO_2.

The seasonality of biomass burnings might explain the plumes of CO_2 observed by IASI exiting central Africa through the west coast in boreal winter, and exiting southern Africa and America in summer. Fire activity is seasonal, generally lasting 3–4 months according to the dry season length (Duncan et al., 2003; Cooke et al., 1996). In southern

Africa, the fire season extends from April to October and shows a peak in June–July; in northern Africa, the fire season extends from November to April, and shows a maximum in December-January (Cahoon et al., 1992; Barbosa et al., 1999; Chédin et al., 2008). In South America, the fire seasonality is weaker than in Africa and shows a peak in August for southern South America and in January for northern South America (Hoelzemann et al., 2004). From July to September, a maximum of CO_2 concentration is found East of Africa over the Pacific. This strong signature, already found with AIRS observations (Crevoisier et al., 2004), might be due to two effects: biomass burning emission from southern Africa, and pollution from Asia migrating to this region. The observed variability is partly yet not fully understood and more work needs to be done to fully understand the retrieved spatio-temporal distribution.

As compared to several atmospheric transport model simulations previously published with the aim of evaluating CO_2 fields derived from thermal infrared observations (Tiwari et al., 2005; Chevallier et al., 2005), IASI shows a much higher variability than any model simulations, which are usually characterized by a strong latitudinal structure. This might be explained by the difficulty of models to reproduce vertical transport to the upper troposphere (Tiwari et al., 2006; Shia et al., 2006; Yang et al., 2007; Stephens et al., 2007). Together with other instruments, IASI should provide a means to observe and understand atmospheric transport pathways of CO_2 from the surface to the upper troposphere.

In the absence of observed global maps of tropospheric CO_2, a first way of quantifying the dispersion of the retrievals is to determine the standard deviation of each monthly $5^\circ \times 5^\circ$ box item sample. A small dispersion of $\sim$2.7 ppmv is observed (less than 1% of the mean CO_2 mixing ratio), which partly comes from the errors due to the method and to the instrument, and partly from the natural variability of CO_2 within each box over one month. The smallest values of the standard deviation ($\sim$2.2 ppmv) correspond to the months of October–November when the natural variability (and the concentration, in particular in the northern tropics) is at its minimum, and the maximum values ($\sim$3.1 ppmv) correspond to the months of June–August when the natural variability (and the concentration, in particular in the northern tropics) is at its maximum. Following Chédin et al. (2003), these standard deviations may tentatively be seen as resulting from the combination of the standard deviation of the method (σ_M) itself and of the standard deviation of the natural variability (σ_V) of CO_2 ($5^\circ \times 5^\circ$, one month). Doing so, σ_M comes to about 2.0 ppmv ($\sim$0.5%) and σ_V comes to 1.0 ppmv in October–November and to 2.4 ppmv in June–August. Such numbers look reasonable. However, this result is more an appreciation of the internal consistency of the method than an estimation of its precision. Associated with the comparison to in situ measurements these values bring some confidence in the overall description of the features of the CO_2 field variability.

5 Conclusions

With its high spectral resolution, IASI, coupled with AMSU microwave observations, provides new capabilities to monitor carbon dioxide in the troposphere. Fourteen channels, located in band ν_2 of CO_2 near 15 μm, present high sensitivities to CO_2 and no sensitivity to water vapor, ozone and surface characteristics. They are mostly sensitive to CO_2 variations in the upper troposphere, thus leading to the retrieval of an upper tropospheric integrated content representative of the 11–15 km range in the tropics through the use of a non-linear inference scheme based on neural networks. The high radiometric noise affecting IASI channels in the shortwave precludes using this spectral region to retrieve CO_2, thus yielding a sensitivity to CO_2 variations at higher altitudes than for AIRS.

It is worth noting that the IASI CO_2 retrieval scheme does not use any a priori information on the trend, the seasonality, nor the geographical distribution of carbon dioxide. Likewise, the IASI CO_2 retrievals are fully independent from any a priori knowledge of the state of the atmosphere and do not rely on any Level 2 data. To separate the radiative effects of temperature and CO_2, which is the core of the ability of infrared sounders to measure CO_2 variations, use is made of observations performed simultaneously by IASI, sensitive to both temperature and CO_2, and AMSU, only sensitive to temperature. The performance of the retrieval is thus linked to both IASI and AMSU instruments. The precision of the retrievals has been found to be about 2 ppmv ($\sim$0.5%), for a $5^\circ \times 5^\circ$ spatial resolution on a monthly time scale. However, a direct estimation of their precision is not possible due to lack of direct simultaneous measurements.

In terms of seasonality and latitudinal variation, the retrievals, performed for clear-sky only, agree well with in-situ measurements performed in the mid-troposphere in the past few years. However, the cycle retrieved from IASI (with maximum sensitivity at 13 km) is lagged backward by two months as compared to the surface, lagged backward by one month as compared to measurements performed at 11 km and to retrievals from AIRS which has a maximum sensitivity at 11 km, and lagged forward by one month as compared to observations performed at the tropopause (16 km). This is likely due to vertical transport of CO_2 cycle, and might prove useful to better understand the evolution of the phasing of CO_2 seasonal cycle with altitude.

The retrieved spatial variations have highlighted latitudinal and longitudinal CO_2 variations which could be attributed to surface emissions uplifted to the upper troposphere. Therefore, IASI retrievals potentially bring additional information on the detection of atmospheric transport pathways and on the mechanisms that transport CO_2 emissions from the surface to the upper atmosphere. Even if not sensitive to surface CO_2, IASI observations might thus prove useful for constraining atmospheric transport in a so-called surface flux inversion. However, while performing any

estimate of sources and sinks, it is required to take into account the fact that retrievals are only performed in clear-sky conditions. With the launch of two other successive IASI-like instruments, scheduled for 2011 and 2015, more than 20 years of CO_2 will be available for climate studies.

Acknowledgements. This work has been supported in part by the European Community under the contract FP6-516099 ("GEMS"). We particularly wish to thank Cathy Boone and the Ether center team for their help in getting IASI data, and the two anonymous referees for their supportive comments and suggestions. IASI has been developed and built under the responsibility of the Centre National d'Etudes Spatiales (CNES, France). It is flown onboard the Metop satellites as part of the EUMETSAT Polar System. The IASI L1 data are received through the EUMETCast near real time data distribution service.

Edited by: A. Richter

The publication of this article is financed by CNRS-INSU.

References

Barbosa, P. M., Stroppiana, D., Grégoire, J. M., and Pereira, J. M. C.: An assessment of vegetation fire in Africa (1981–1991): Burned areas, burned biomass, and atmospheric emissions, Global Biogeochem. Cy., 13, 933–950, 1999.

Barkley, M. P., Monks, P. S., Hewitt, A. J., Machida, T., Desai, A., Vinnichenko, N., Nakazawa, T., Yu Arshinov, M., Fedoseev, N., and Watai, T.: Assessing the near surface sensitivity of SCIAMACHY atmospheric CO_2 retrieved using (FSI) WFM-DOAS, Atmos. Chem. Phys., 7, 3597–3619, 2007, http://www.atmos-chem-phys.net/7/3597/2007/.

Boering, K. A., Wofsy, S. C., Daube, B. C., Schneider, J. R., Loewenstein, M., Podolske, J. R., and Conway, T. J.: Stratospheric mean ages and transport rates from observations of CO_2 and N_2O , Science, 274, 1340–1343, 1996.

Buchwitz, M., de Beek, R., Burrows, J. P., Bovensmann, H., Warneke, T., Notholt, J., Meirink, J. F., Goede, A. P. H., Bergamaschi, P., Körner, S., Heimann, M., and Schulz, A.: Atmospheric methane and carbon dioxide from SCIAMACHY satellite data: initial comparison with chemistry and transport models, Atmos. Chem. Phys., 5, 941–962, 2005, http://www.atmos-chem-phys.net/5/941/2005/.

Cahoon, D. R., Stocks, B. J., Levine, J. S., Coter III, W. R., and O'Neill, C. P.: Seasonal distribution of African savanna fires, Nature, 359, 812–815, 1992.

Chahine, M. T., Barnet, C. D., Olsen, E. T., Chen, L., and Maddy, E.: On the determination of atmospheric minor gases by the method of vanishing partial derivatives with application to CO_2, Geophys. Res. Lett., 32, L22803, doi:10.1029/2005GL024165, 2005.

Chahine M. T., Chen, L., Dimotakis, P., Jiang, X., Li, Q., Olsen, E. T., Pagano, T., Randerson, J., and Yung, Y. L.: Satellite remote sounding of mid-tropospheric CO_2, Geophys. Res. Lett., 35, L17807, doi:10.1029/2008GL035022, 2008.

Chédin, A., Scott, N. A., Wahiche, C., and Moulinier, P.: The improved initialisation inversion method: A high resolution physical method for temperature retrievals from satellites of the TIROS-N series, J. Clim. Appl. Meteorol., 24, 128–143, 1985.

Chédin, A., Hollingsworth, A., Scott, N. A., Serrar, S., Crevoisier, C., and Armante, R.: Annual and seasonal variations of atmospheric CO_2, N_2O, and CO concentration retrieved from NOAA/TOVS satellite observations, Geophys. Res. Lett., 29(8), 1269, doi:10.1029/2001GL014082, 2002.

Chédin, A., Serrar, S., Scott, N. A., Crevoisier, C., and Armante, R.: First global measurement of mid-tropospheric CO_2 from NOAA polar satellites: Tropical zone, J. Geophys. Res., 108(D18), 4581, doi:10.1029/2003JD003439, 2003.

Chédin, A., Scott, N. A., Armante, R., Pierangelo, C., Crevoisier, C., Fossé, O., and Ciais, P.: A quantitative link between CO_2 emissions from tropical vegetation fires and the daily tropospheric excess (DTE) of CO_2 seen by NOAA-10 (1987–1991), J. Geophys. Res., 113, D05302, doi:10.1029/2007JD008576, 2008.

Chevallier, F., Engelen, R. J., and Peylin, P.: The contribution of AIRS data to the estimation of CO_2 sources and sinks, Geophys. Res. Lett., 32, L23801, doi:10.1029/2005GL024229, 2005.

Cooke, W., Koffi, B., and Grégoire, J. M.: Seasonality of vegetation fires in Africa from remote sensing data and application to a global chemistry model, J. Geophys. Res., 101, 21051–21065, 1996.

Crevoisier, C., Chédin, A., and Scott, N. A., AIRS channel selection for CO_2 and other trace-gas retrievals, Q. J. Roy. Meteorol. Soc., 129, 2719–2740, 2003a.

Crevoisier, C., Chédin, A., Heilliette, S., Scott, N. A., Serrar, S., Armante, R.: Mid-tropospheric CO_2 retrieval in the tropical zone from AIRS observations, Proceedings of the 13th International TOVS Study Conference, 2003b.

Crevoisier C., Heilliette, S., Chédin, A., Serrar, S., Armante, R., and Scott, N. A.: Midtropospheric CO_2 concentration retrieval from AIRS observations in the tropics, Geophys. Res. Lett., 31, L17106, doi:10.1029/2004GL020141, 2004.

Crevoisier, C., Nobileau, D., Fiore, A. M., Armante, R., Chédin, A., and Scott, N. A.: A new insight on tropospheric methane in the Tropics – first year from IASI hyperspectral infrared observations, Atmos. Chem. Phys. Discuss., 9, 6855–6887, 2009, http://www.atmos-chem-phys-discuss.net/9/6855/2009/.

Duncan, B. N., Martin, R. V., Staudt, A. C., Yevich, R., and Logan, J. A.: Interannual and seasonal variability of biomass burning emissions constrained by satellite observations, J. Geophys. Res., 108(D2), 4100, doi:10.1029/2002JD002378, 2003.

Engelen, R. J., Andersson, E., Chevallier, F., Hollingsworth, A., Matricardi, M., McNally, A. P., Thépaut, J.-N., and Watts, P. D.: Estimating atmospheric CO_2 from advanced infrared satellite radiances within an operational four-dimensional variational (4D-Var) data assimilation system: Methodology and first results, J. Geophys. Res., 109, D19309, doi:10.1029/2004JD004777, 2004.

Engelen, R. J., and McNally, A. P.: Estimating atmospheric CO_2 from advanced infrared satellite radiances within an op-

erational fourdimensional variational (4D-Var) data assimilation system: Results and validation, J. Geophys. Res., 110, D18305, doi:10.1029/2005JD005982, 2005.

Engelen, R. J., Serrar, S., and Chevallier, F.: Four-dimensional data assimilation of atmospheric CO_2 using AIRS observations, J. Geophys. Res., 114, D03303, doi:10.1029/2008JD010739, 2009.

GLOBALVIEW-CO_2: Cooperative Atmospheric Data Integration Project – Carbon Dioxide. CD-ROM, NOAA ESRL, Boulder, Colorado (also available on Internet via anonymous FTP to ftp.cmdl.noaa.gov, Path: ccg/co2/GLOBALVIEW), 2008.

Gurney, K. R., Law, R. M., Denning, A. S., Rayner, P. J., Pak, B., and TransCom 3 L2 modelers: Transcom 3 Inversion Intercomparison: model mean results for the estimation of seasonal carbon sources and sinks, Global Biogeochem. Cy., 18, GB1010, doi:10.1029/2003GB002111, 2004.

Jacquinet-Husson, N., Scott, N. A., Chédin, A., Crépeau, L., Armante, R., Capelle, V., and 47 co-authors: The GEISA spectroscopic database: Current and future archive for Earth and planetary atmosphere studies, J. Quant. Spectrosc. Ra., 109, 1043–1059, 2008.

Hoelzemann, J. J., Schultz, M. G., Brasseur, G. P., Granier, C., and Simon, M.: The Global Wildland fire Emission Model GWEM: Evaluating the use of global area burnt satellite data, J. Geophys. Res., 109, D14S04, doi:10.1029/2003JD003666, 2004.

Houweling, S., Hartmann, W., Aben, I., Schrijver, H., Skidmore, J., Roelofs, G.-J., and Breon, F.-M.: Evidence of systematic errors in SCIAMACHY-observed CO_2 due to aerosols, Atmos. Chem. Phys., 5, 3003–3013, 2005, http://www.atmos-chem-phys.net/5/3003/2005/.

Machida, T., Matsueda, H., and Sawa, Y.: A new JAL project: CONTRAIL - Comprehensive Observation Network for Trace gases by AIrLiner, IGAC Newsletter, 37, 23–30, 2007.

Machida, T., Matsueda, H., Sawa, Y., Nakagawa, Y., Hirotani, K., Kondo, N., Goto, K., Nakazawa, T., Ishikawa, K., and Ogawa, T.: Worldwide measurements of atmospheric CO_2 and other trace gas species using commercial airlines, J. Atmos. Ocean. Tech., 25(10), 1744–1754, doi:10.1175/2008JTECHA1082.1, 2008.

Maddy, E. S., Barnet, C. D., Goldberg, M., Sweeney, C., and Liu, X.: CO_2 retrievals from the Atmospheric Infrared Sounder: Methodology and validation, J. Geophys. Res., 113, D11301, doi:10.1029/2007JD009402, 2008.

Matsueda, H., Inoue, H., and Ishii, M.: Aircraft observation of carbon dioxide at 8–13 km altitude over the western Pacific from 1993 to 1999, Tellus B, 54, 1–21, 2002.

Matsueda, H., Machida, T., Sawa, Y., Nakagawa, Y., Hirotani, K., Ikeda, H., Kondo, N., and Goto, K.: Evaluation of atmospheric CO_2 measurements from new flask air sampling of JAL airliner observation, Pap. Meteorol. Geophys., 59, 1–17, 2008.

Nakazawa, T., Miyashita, K., Aoki, S., and Tanaka, M.: Temporal and spatial variations of upper troposphere and lower stratospheric carbon dioxide, Tellus, 43B, 106–117, 1991.

Rumelhart, D. E., Hinton, G. E., and Williams, R. J.: Learning internal representations by error propagation, in: Parallel Distributed Processing: Explorations in the Macrostructure of Cognition, vol. 1, edited by: Rumelhart, D. E. and McClelland, J. L., MIT Press, Cambridge, Mass, 318-362, 1986.

Sawa, Y., Machida, T., and Matsueda, H.: Seasonal variations of CO_2 near the tropopause observed by commercial aircraft, J. Geophys. Res., 113, D23301, doi:10.1029/2008JD010568, 2008.

Scott, N. A. and Chédin, A.: A fast line-by-line method for atmospheric absorption computations: The Automatized Atmospheric Absorption Atlas, J. Appl. Meteorol., 20, 556–564, 1981.

Schneising, O., Buchwitz, M., Burrows, J. P., Bovensmann, H., Reuter, M., Notholt, J., Macatangay, R., and Warneke, T.: Three years of greenhouse gas column-averaged dry air mole fractions retrieved from satellite – Part 1: Carbon dioxide, Atmos. Chem. Phys., 8, 3827–3853, 2008, http://www.atmos-chem-phys.net/8/3827/2008/.

Shia, R. L., Liang, M. C., Miller, C. E., and Yung, Y. L.: CO_2 in the upper troposphere: Influence of stratosphere-troposphere exchange, Geophys. Res. Lett., 33, L14814, doi:10.1029/2006GL026141, 2006.

Stephens, B. B., Gurney, K. R., Tans, P. P., Sweeney, C., Peters, W., Bruhwiler, L., Ciais, P., Ramonet, M., Bousquet, P., Nakazawa, T., et al.: Weak northern and strong tropical land carbon uptake from vertical profiles of atmospheric CO_2, Science, 316, 1732–1735, 2007.

Strahan, S., Douglass, A., Nielsen, J., and Boering, K.: The CO_2 seasonal cycle as a tracer of transport, J. Geophys. Res., 103(D12), 13729–13741, 1998.

Strahan, S. E., Duncan, B. N., and Hoor, P.: Observationally derived transport diagnostics for the lowermost stratosphere and their application to the GMI chemistry and transport model, Atmos. Chem. Phys., 7, 2435–2445, 2007, http://www.atmos-chem-phys.net/7/2435/2007/.

Strow, L. L. and Hannon, S. E.: A 4-year zonal climatology of lower tropospheric CO_2 derived from ocean-only Atmospheric Infrared Sounder observations, J. Geophys. Res., 113, D18302, doi:10.1029/2007JD009713, 2008.

Tans, P. P., Fung, I. Y., and Takahashi, T.: Observational constraints on the global atmospheric CO_2 budget, Science, 247, 1431–1438, 1990.

Tiwari, Y. K., Gloor, M., Engelen, R. J., Chevallier, F., Rodenbeck, C., Korner, S., Peylin, P., Braswell, B. H., and Heimann, M.: Comparing CO_2 retrieved from Atmospheric Infrared Sounder with model predictions: Implications for constraining surface fluxes and lower-to-upper troposphere transport, J. Geophys. Res., 111, D17106, doi:10.1029/2005JD006681, 2006.

Turner, D. S.: The effect of increasing CO_2 amounts on TOVS longwave sounding channels, J. Appl. Meteorol., 32, 1760–1766, 1993.

Turner, D. S.: HIRS sensitivity to CO_2 mixing ratio and a pragmatic correction term, J. Appl. Meteorol., 33, 1155–1162, 1994.

Yang, Z., Washenfelder, R. A., Keppel-Aleks, G., Krakauer, N. Y., Randerson, J. T., Tans, P. P., Sweeney, C., and Wennberg, P. O.: New constraints on Northern Hemisphere growing season net flux, Geophys. Res. Lett., 34, L12807, 2007.